

# Design of Compact Transversal Wideband Bandpass Filter with Wide Upper Stopband

Li-Tian Wang<sup>1</sup>, Yang Xiong<sup>2, \*</sup>, Wan-Jing Wang<sup>1</sup>, Li Gong<sup>1</sup>,  
Zhao Li<sup>1</sup>, Xia-Qing Li<sup>1</sup>, and Zhe-Long Liang<sup>1</sup>

**Abstract**—A compact wideband bandpass filter (BPF) with stopband suppression by utilizing transversal signal interaction concepts is proposed in this article. Two transmission paths from Port I to Port II are separately constructed by multi-mode step impedance resonator (SIR) and shorted coupled lines. The proposed configuration generates two controllable transmission poles, and wideband characteristic can be realized. Moreover, multiple transmission zeros are implemented by signals superposition of two transmission paths and stub loaded fans resulting in steepness sideband and broad upper stopband suppression up to 100 GHz. For clarification, the designed wideband centered at 4.5 GHz with fractional bandwidth of 14.2% is designed, assembled and measured. The circuit size of prototype BPF only occupies 0.94 cm<sup>2</sup>, and the presented BPF is evaluated by test results and simulated predictions with good agreement.

## 1. INTRODUCTION

In modern radio frequency (RF) telecommunication systems, planar bandpass filters (BPFs) have become indispensable key block in RF front design due to their compact size, simple structures, and easy production [1]. With continuous development of communication protocols, numerous unwanted interference bands present challenges to the design of BPFs. To suppress spurious interferences, the planar BPFs with extended stopband have aroused tremendous attention and extensively investigated.

As a conventional method, BPFs with transmission zeros (TZs) can be obtained based on multi-mode resonator (MMR) [2–6]. In [3], a 0° feeding structure is introduced to yield TZs in the design of BPFs with high selectivity and stopband attenuation. A wideband BPF is also obtained by employing a quad mode resonator [5], and the presented BPF has advantages of miniaturized circuit size, four TZs, and high selectivity while the center frequency (CF) is uncontrollable, and stopband needs to be further extended. To approach BPFs with wide out-of-band suppression, multiple methods can be utilized to push the harmonics to higher frequency, such as step impedance resonators (SIRs) [7–9] and interdigital structure resonators [10]. Owing to the merits of SIR for shifting harmonic, a wide stopband BPF with multiple TZs is realized with the flaw of relative large size in [7]. In [8], a BPF with independently controllable CF of passbands is based on a coupled asymmetric SIR configuration. For size reduction consideration, wideband BPF with compact size can be constructed by utilizing a multi-layer structure, but at the expense of raised fabrication difficulties [11, 12]. High temperature superconductor with low surface resistance is applied to obtain BPF in [13]. For this method, the implemented BPF is of sharp sideband steepness and high suppression level of stopband. Recently, the parallel coupled line (PCL) structure has become a candidate and exclusively demonstrated for BPF design since its unique transmission characteristics [14–16]. In [15], a wideband BPF with fractional bandwidth ( $fbw$ ) of

---

Received 10 January 2020, Accepted 1 July 2020, Scheduled 5 September 2020

\* Corresponding author: Yang Xiong (xiongyang0291@163.com).

<sup>1</sup> College of Electronic Information and Optical Engineering, Nankai University, Tianjin 300350, P. R. China. <sup>2</sup> Southwest China Institute of Electronic Technology, Chengdu 610036, P. R. China.

60% is exploited, and the BPF has merits of multiple TZs and out-of-band suppression without spurious notches. Furthermore, transversal signal interaction (TSI) techniques have attracted much attention for wideband BPF designing [17, 18]. By using this method, multiple TZs can be generated by signal energy cancellations of two signal transmission paths, and wide band with sharp skirts and wide stopband can be therefore implemented. Nevertheless, the stopband bandwidths of aforementioned BPFs are still insufficient.

The primary motivation of this article is to design a miniaturized wideband BPF with wide stopband extended to 100 GHz. Thereby, such a BPF can be applied in the new generation of telecommunication networks. In this paper, a transversal BPF is developed with two transmission paths which respectively consist of a multi-mode SIR and shorted anti-coupled line structure. In the rejection band realization, the TSI concepts, SIR, and stub loaded fans are adapted to develop wide stopband suppression up to 100 GHz. In addition, the proposed wideband BPF is designed with miniaturized circuit size ( $0.94 \text{ cm}^2$ ), independently controllable CF, high selectivity, and multiple TZs. The detailed design methodology is proposed and demonstrated. For verification, the proposed compact wideband BPF is analyzed, implemented, and tested. The simulated prediction and measured results have been discussed.

## 2. TRANSVERSAL BPF DESIGN

Figure 1 depicts the geometrical layout of proposed BPF. It can be observed that there are two signal transmission paths from Port I to Port II. For path 1<sup>st</sup> (Path I), a pair of multi-mode SIRs with identical physical dimension parameters  $((L_1, W_1), (L_2, W_2), (L_3, W_3))$  is connected by a shorted stub (denoted by  $(L_4, W_4)$ ), and  $R_1$  is the radius of the via hole. Meanwhile, a shorted anti-coupled lines structure (denoted by  $(L_5, W_5, g)$ ) is constructed for path 2<sup>nd</sup> (Path II). Plus, two  $30^\circ$  fan stubs with radii of  $R_2$  and  $R_3$  are loaded at the input feeding line and output feeding line, respectively. The ideal transmission line model (TLM) of the TSI is demonstrated in Fig. 2, where  $\theta_n$  ( $n = 1, 2, 3, 4$ , and  $5$ ) and  $Z_i$  ( $i = 1, 2, 3$  and  $4$ ) respectively stand for electrical lengths and characteristic impedances of corresponding microstrip line. The theoretical analysis of the presented TLM model can be carried out by employing  $ABCD$  matrix. The  $ABCD$  matrices of the microstrip transmission lines in path 1<sup>st</sup> (Path I) can be

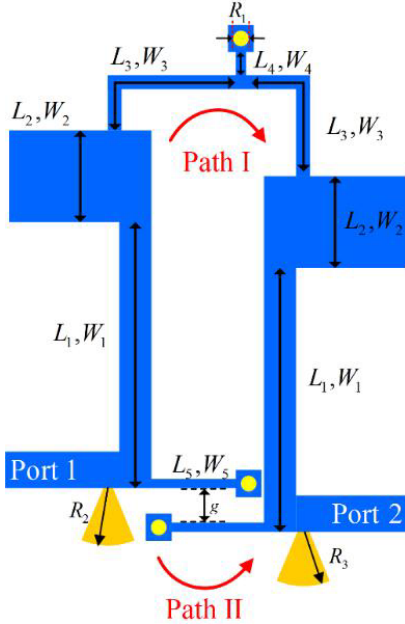


**Figure 1.** Physical layout of the prototype TSI BPF.

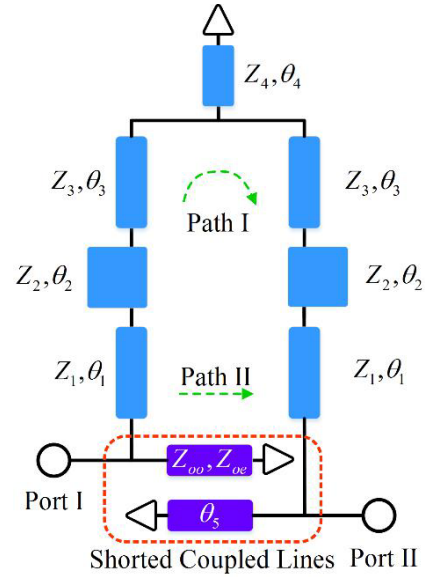


**Figure 2.** The ideal equivalent circuit configuration of proposed BPF.

expressed as:

$$M_{Li} = \begin{bmatrix} \cos \theta_i & jZ_i \sin \theta_i \\ jY_i \sin \theta_i & \cos \theta_i \end{bmatrix} \quad (i = 1, 2 \text{ and } 3)$$

$$M_{L4} = \begin{bmatrix} 1 & 0 \\ -jY_4 \cot \theta_4 & 1 \end{bmatrix}$$

where  $M_{Li}$  ( $i = 1, 2, 3$ , and 4) represents the  $ABCD$  matrix of the counterpart microstrip line with characteristic impedance  $Z_i$  ( $i = 1, 2, 3$ , and 4), and  $Y_i = Z_i$  denote the characteristic admittances. Thereby, the  $ABCD$  matrix of path 1<sup>st</sup> (Path I),  $M_{\text{pathI}}$ , can be calculated by

$$M_{\text{pathI}} = \begin{bmatrix} A_1 & B_1 \\ C_1 & D_1 \end{bmatrix} = M_{L1} \times M_{L2} \times M_{L3} \times M_{L4} \times M_{L3} \times M_{L2} \times M_{L1}$$

Afterward, we convert the  $ABCD$  matrix of path 1<sup>st</sup> (Path I) to  $Y$  matrix as below:

$$Y_{\text{pathI}} = \begin{bmatrix} Y_{11}^1 & Y_{12}^1 \\ Y_{21}^1 & Y_{22}^1 \end{bmatrix} = \begin{bmatrix} \frac{D_1}{B_1} & \frac{B_1 C_1 - A_1 D_1}{B_1} \\ -\frac{1}{B_1} & \frac{A_1}{B_1} \end{bmatrix}$$

For transmission path 2<sup>nd</sup> (Path II), the  $Y$  matrix of shorted anti-PCL can be written as [12]:

$$Y_{\text{pathII}} = \begin{bmatrix} Y_{11}^2 & Y_{12}^2 \\ Y_{21}^2 & Y_{22}^2 \end{bmatrix} = \begin{bmatrix} -j \frac{Y_{oe} + Y_{oo}}{2} \cot \theta_5 & -j \frac{Y_{oe} - Y_{oo}}{2} \csc \theta_5 \\ -j \frac{Y_{oe} - Y_{oo}}{2} \csc \theta_5 & -j \frac{Y_{oe} + Y_{oo}}{2} \cot \theta_5 \end{bmatrix}$$

Then the  $Y$  matrix of the presented ideal TLM structure can be demonstrated as:

$$Y = Y_{\text{pathI}} + Y_{\text{pathII}} = \begin{bmatrix} Y_{11}^1 + Y_{11}^2 & Y_{12}^1 + Y_{12}^2 \\ Y_{21}^1 + Y_{21}^2 & Y_{22}^1 + Y_{22}^2 \end{bmatrix} = \begin{bmatrix} Y_{11} & Y_{12} \\ Y_{21} & Y_{22} \end{bmatrix}$$

herein,

$$\begin{cases} Y_{11} = \frac{D}{B} - j \frac{Y_{oe} + Y_{oo}}{2} \cot \theta_5 \\ Y_{12} = \frac{BC - AD}{B} - j \frac{Y_{oe} - Y_{oo}}{2} \csc \theta_5 \\ Y_{21} = -\frac{1}{B} - j \frac{Y_{oe} - Y_{oo}}{2} \csc \theta_5 \\ Y_{22} = \frac{A}{B} - j \frac{Y_{oe} + Y_{oo}}{2} \cot \theta_5 \end{cases}$$

By employing transformation from  $Y$ -parameters to  $ABCD$ -parameters, thus transmission coefficient ( $S_{21}$ ) and reflection coefficient ( $S_{11}$ ) can be derived as [19]:

$$S_{21} = -\frac{2Y_{21}Y_0}{\Delta Y}$$

$$S_{11} = \frac{(Y_0 - Y_{11})(Y_0 + Y_{22}) + Y_{12}Y_{21}}{\Delta Y}$$

herein,  $\Delta Y$  is defined as  $\Delta Y = (Y_{11} + Y_0)(Y_{22} + Y_0) - Y_{12}Y_{21}$ ,  $Y_0 = 0.02 \text{ S}$  and  $Z_0 = 1/Y_0 = 50 \Omega$  is characteristic impedances of two feeding lines at the input port and output port. For calculation simplicity, the initial parameters are assumed as  $\theta_1 = 2\theta_3$ ,  $\theta_3 = 2\theta_2$ ,  $\theta_2 = 2\theta_4$ ,  $\theta_3 = 30^\circ$ ,  $\theta_5 = 10^\circ$ ,  $Z_3 = Z_4 = Z_5 = 100 \Omega$ ,  $K_1 = \frac{Z_1}{Z_3}$ , and  $K_2 = \frac{Z_2}{Z_3}$ , where  $Z_5$  is characteristic impedance of shorted anti PCL, and  $K_1$  and  $K_2$  are impedance ratios of SIR for BPF design. The initial reference frequency  $f_0$  for electrical lengths calculation is set as 4.5 GHz, i.e., the CF of the BPF. When  $S_{21} = 1$  is satisfied, the numerical solution of transmission poles can be extracted by means of MATLAB. Therefore, two

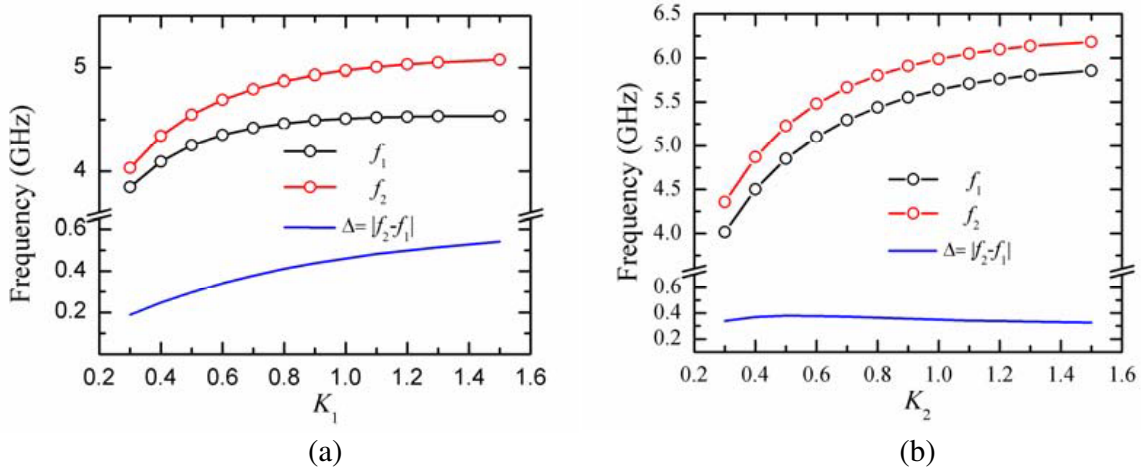


**Figure 3.** Design graph for proposed TSI wideband BPF. (a) Resonant modes and absolute bandwidth versus impedance ratio  $K_1$ , (b) resonant modes and absolute bandwidth versus impedance ratio  $K_2$ .

numerical solutions, i.e., resonant modes  $f_1$  and  $f_2$ , can be derived in neighborhoods of designed passband. Two resonant frequencies are illustrated with respect to varied  $K_1$  and  $K_2$ , respectively in Fig. 3(a) and Fig. 3(b). The absolute bandwidth of the BPF is defined as  $\Delta = |f_2 - f_1|$ . It can be seen from Fig. 3(a) that  $f_1$  and  $f_2$  enlarge with the increase of  $K_1$ . Meanwhile, the bandwidth gets larger as  $K_1$  increases. As sketched in Fig. 3(b),  $f_1$  and  $f_2$  are raised with enlargement of  $K_2$ , whereas the variation of  $K_2$  has minor effect on bandwidth.

To investigate the effect of PCL on resonant frequencies, the resonant modes  $f_1$  and  $f_2$  with varied  $k$  and  $\theta_5$  are plotted in Fig. 6. Here  $k$  is the normalized coupling strength of shorted anti PCL, and  $k$  can be formulated from

$$k = \frac{Z_{oe} - Z_{oo}}{Z_{oe} + Z_{oo}}$$

herein,  $Z_{oe}$  and  $Z_{oo}$  respectively denote the characteristic impedance of one wire to ground with equal currents in the same direction and characteristic impedance of one wire to ground with equal currents in opposite directions [20]. In Fig. 6, blue lines correspond to fixed values of  $\theta_5$  with various coupling coefficients  $k$ , and the rainbow-colored lines represent the frequencies of resonant modes with fixed value of  $k$  and tuned electrical lengths  $\theta_5$ . As can be derived from Fig. 4,  $f_1$  and  $f_2$  both decline as  $\theta_5$  increases

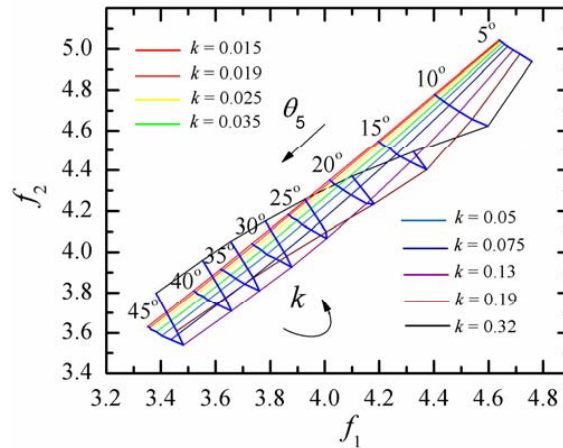


**Figure 4.** Resonant frequencies  $f_1$  and  $f_2$  against different  $\theta_5$  and  $k$  with condition of specified  $K_1 = 0.35$  and  $K_2 = 0.65$ .

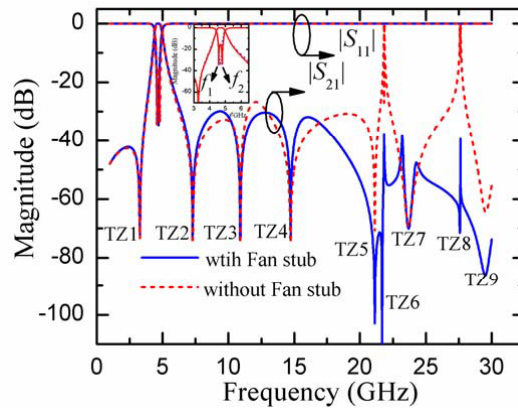


**Figure 5.** Comparison between simulated frequency responses of proposed BPF with fan stub and BPF without fan stub.

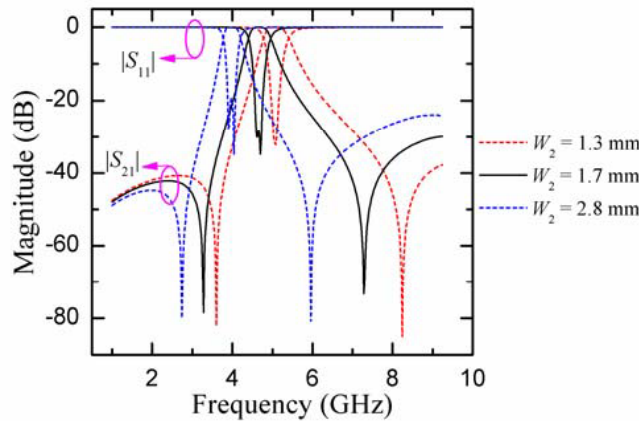


**Figure 6.** Properties of frequency responses versus varied value of  $W_2$ .

with a fixed value of  $k$ . When the normalized coupling coefficient  $k$  is less than 0.13, the lower  $k$  leads to higher frequency of  $f_2$  while the variation of  $k$  has a slight effect on  $f_1$ . Hence, by appropriately selecting the value of  $K_1$ ,  $K_2$ ,  $\theta_5$ , and  $k$ , the design specification of centre frequency and bandwidth can be roughly fulfilled. It is noted that the coupling coefficient of filter can be further managed by fine tuning the value of electrical length  $\theta_4$ .

Therefore, initial frequency responses with properly selected parameters without fan stubs are illustrated by the red short dash lines in Fig. 5. Herein, two spurious harmonics occur at 21.84 GHz and 27.58 GHz, respectively. To attenuate the spurious passbands, two stub loaded fans with radii of  $R_2$  and  $R_3$  are introduced respectively at input port and output port.

When input impedance of fan stub is equal to zero at a certain frequency, a virtual ground is introduced to short out the transmission signal from Port I to Port II, thus a TZ will be planted at this frequency. By appropriately tuning the radius of two stub loaded fans, the transmission characteristics with extended upper stopband suppression can be realized as portrayed in Fig. 5. Meanwhile, the frequency responses within passband are unaffected by the implementation of fan stubs.

As depicted in Fig. 5, The generation mechanism of TZ1, TZ2, TZ3, TZ4, TZ5, TZ7, and TZ9 is that the phase difference of path 1<sup>st</sup> (Path I) and path 2<sup>nd</sup> (Path II) is  $(2n + 1)\pi$ ; destructive interference occurs between two paths; and a TZ will be generated finally.

Moreover, two fan stub loaded structure shorts out the specific frequency when input impedance of each fan stub is zero at TZ6 and TZ8.

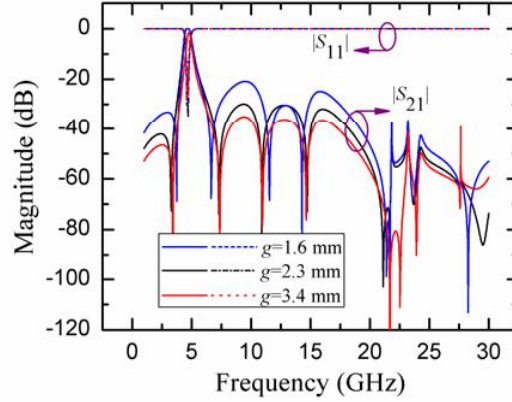


**Figure 7.** The simulated results with varied value of  $g$ .

Furthermore, the CF of proposed BPF can be independently controllable by adjusting the value of  $W_2$ . The CF shifts toward lower frequency with increasing value of  $W_2$ , and the return loss of passband is better than 20 dB within the manageable range, as shown in Fig. 6. Furthermore, by properly changing the value of  $g$ , the suppression level of upper stopband can be improved, as demonstrated in Fig. 7. It can be seen from Fig. 7 that the upper stopband attenuation level is improved with higher value of  $g$ . When the value of  $g$  is set as 3.4 mm, the out of band suppression level can reach 35-dB within the range of 6.5 GHz to more than 30 GHz.

### 3. OPTIMIZED SIMULATED RESULTS AND IMPLEMENTATION

Thereby, all the geometrical parameters are optimized by using full-wave EM simulator, and the frequency responses of optimized TSI BPF are demonstrated in Fig. 8. We can see from the figure that numerous TZs are generated, and a wide stopband range from 5.1 to 100 GHz with rejection level of 10-dB is obtained. The EM simulated responses have the insertion loss of 0.3 dB with the return loss of 22 dB.

To verify the proposed analysis and design method, a prototype BPF is designed and fabricated with microstrip techniques. Figure 9 shows a photograph of presented TSI wide stopband BPF before being assembled, and the circuit size only amounts to  $0.94 \text{ cm}^2$  without feeding lines. The designed BPF in this article is implemented on a 0.508 mm-thick substrate Rogers 4003c with relative constant of 3.55 and loss tangent of 0.0027. Physical dimensions of fabricated prototype BPF are as follows:  $L_1 = 7.5$ ,  $L_2 = 1.65$ ,  $L_3 = 3.55$ ,  $L_4 = 0.7$ ,  $L_5 = 1.65$ ,  $W_1 = 0.55$ ,  $W_2 = 3.2$ ,  $W_3 = 0.225$ ,  $W_4 = 0.35$ ,  $W_5 = 0.225$ ,  $g = 1.725$ ,  $R_1 = 0.3$ ,  $R_2 = 1.1$ ,  $R_3 = 1.475$ , and units are all in mm.

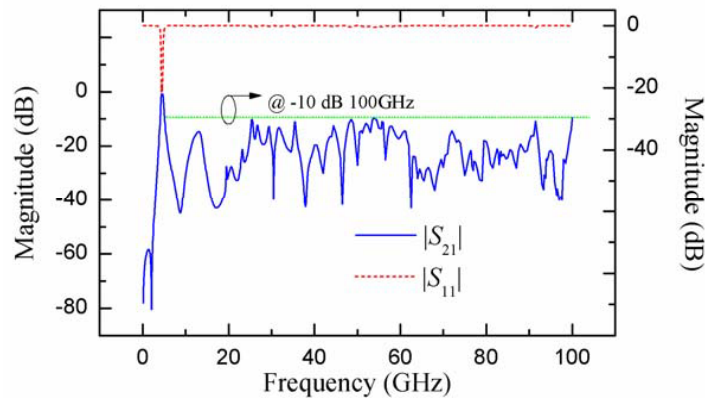


**Figure 8.** Full-wave EM simulation results of presented BPF with wide stopband.

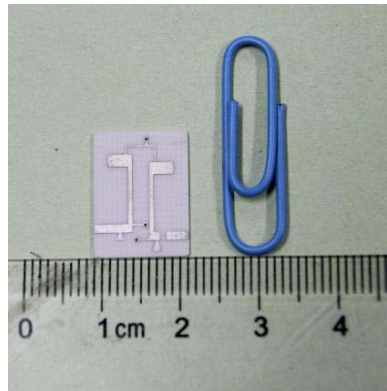


Figure 9. Photograph of proposed wideband TSI BPF under assembled.

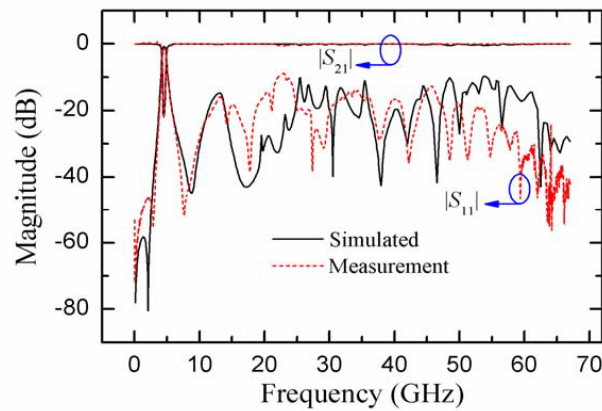


Figure 10. S-parameters of simulated predictions and tested results for designed BPF.

Table 1. Comparison with various pervious works.

Ref.	CFs (GHz)	Fbw (%)	IL (dB)	TZs	Out-band suppression	Circuit Type
[3]	1.4	9.5	1.42	9	11.87 GHz	MMR
[5]	3	43.3	0.6	4	7.59 GHz	MMR
[6]	1.01	11	2	3	6.29 GHz	MMR
[7]	0.415	68.8	1.5	6	3.3 GHz	SIR
[11]	0.96	8	4	4	5.38 GHz	Multi-layer
[13]	0.143	0.99	0.43	0	1.039 GHz	Interdigital
[14]	1.503	10.18	1.28	5	2.46 GHz	PCL
[15]	2.05	60	0.6	8	5.3 GHz	PCL
[17]	1.005	123	0.3	7	5.79 GHz	TSI
<b>This work</b>	<b>4.5</b>	<b>14.2</b>	<b>0.55</b>	<b>&gt; 9</b>	<b>&gt; 100 GHz</b>	<b>PCL, TSI, SIR, Fan stub</b>

Ref: serial number of reference; TZs: number of transmission zeros.

#### 4. RESULTS AND DISCUSSION

The measurement results are characterized by Agilent N5247A vector network analyzer. The comparison of simulated and measured frequency responses are shown in Fig. 10. We can observe that the tested CF is centred at 4.5 GHz with the  $fbw$  of 14.2%. The measured insertion loss (IL) and return loss within the passband are respectively better than 0.55 dB and 14 dB. Furthermore, a wide stopband with an attenuation level of 10 dB is achieved. Additionally, to demonstrate the priority performance of the proposed BPF, a comparison of the proposed BPF and several previous reported works is listed in Table 1. It can be concluded from the table that the proposed miniaturized BPF has advantages in out-of-band performance, which is mainly because the proposed structure integrates various configurations with harmonic suppression such as cascaded SIR, multi-signal transmission path, and fan stub.

#### 5. CONCLUSION

A novel transversal wideband BPF with multi-mode SIR and shorted anti PCL is proposed in this paper. With the presented design methodology, the design specifications of CF and  $fbw$  can be easily approached. Thanks to the presented configuration with transmission signal interaction concepts and fan stubs, multiple TZs are generated, and broad out-of-band suppression can reach 100 GHz. Moreover, the proposed BPF has the advantages of miniaturized circuit size, sharp skirt, and independently controllable CF. The experimental results agree well with simulation predictions, which validates the effectiveness of proposed method.

#### REFERENCES

1. Hong, J. S., "Microstrip filters for RF/microwave applications," *IEEE Microwave Magazine*, Vol. 3, No. 3, 62–65, 2002.
2. Xiong, Y., et al., "Dual-wideband bandpass filter with independently controllable center frequencies and wide stopband," *International Journal of Microwave & Wireless Technologies*, Vol. 10, 93–99, 2018.
3. Li, D., et al., "Compact microstrip bandpass filter with sharp roll-off and broad stopband using modified  $0^\circ$  feed structure," *International Journal of electronic and communications (AEU)*, No. 7, 17–22, 2019.
4. Malherbe, J. A. G., "Wideband bandpass filter with extremely wide upper stopband," *IEEE Transactions on Microwave Theory and Techniques*, Vol. 66, No. 6, 2822–2827, 2018.
5. Huang, J. M., B. Zhang, and S. S. Li, "Novel compact quad-mode wideband bandpass filter with wide stopband using T-shaped resonator," *Journal of Electromagnetic Waves and Applications*, Vol. 28, No. 3, 326–333, 2014.
6. Li, S. and Z. Zhang, "Compact multi-order bandpass filter with high stopband rejection performance," *Electronics Letters*, Vol. 55, No. 12, 701–703, Jun. 13, 2019.
7. Tang, C., C. Tseng, S. Chiu, and P. Wu, "Design of wide passband/stopband microstrip bandpass filters with the stepped coupled line," *IEEE Transactions on Microwave Theory and Techniques*, Vol. 61, No. 3, 1095–1103, Mar. 2013.
8. Kim, C. H. and K. Chang, "Independently controllable dual-band bandpass filters using asymmetric stepped-impedance resonators," *IEEE Transactions on Microwave Theory and Techniques*, Vol. 59, No. 12, 3037–3047, 2011.
9. Zhang, Z., Q. Yang, and Y.-C. Jiao, "Dual-wideband BPF with wide upper stopband using shorted stepped-impedance stub-loaded lowpass filter," *Electronics Letters*, Vol. 52, No. 19, 1615–1616, 2016.
10. Belyaev, B. A., A. M. Serzhantov, A. A. Leksikov, Y. F. Bal'va, and A. A. Leksikov, "Novel high-quality compact microstrip resonator and its application to bandpass filter," *IEEE Microwave and Wireless Components Letters*, Vol. 25, No. 9, 579–581, Sep. 2015.
11. Ta, H. H. and A. Pham, "Compact wide stopband bandpass filter on multilayer organic substrate," *IEEE Microwave and Wireless Components Letters*, Vol. 24, No. 3, 161–163, Mar. 2014.

12. Chen, J. X., et al., "Compact multi-layer bandpass filter with wide stopband using selective feeding scheme," *IEEE Transactions on Circuits & Systems II Express Briefs*, Vol. 65, No. 8, 1009–1013, 2018.
13. Wang, D., B. Wei, B. Cao, J. Chen, T. Zhen, and T. Gao, "A compact wide stopband HTS filter with ground surrounded quasi-interdigital structures," *IEEE Microwave and Wireless Components Letters*, Vol. 25, No. 11, 703–705, Nov. 2015.
14. Lin, S., "New microstrip cascaded-quadruplet bandpass filter based on connected couplings and short-ended parallel-coupled line," *IEEE Microwave and Wireless Components Letters*, Vol. 24, No. 1, 2–4, Jan. 2014.
15. Xu, K., D. Li, and Y. Liu, "High-selectivity wideband bandpass filter using simple coupled lines with multiple transmission poles and zeros," *IEEE Microwave and Wireless Components Letters*, Vol. 29, No. 2, 107–109, Feb. 2019.
16. Killamsetty, V. K. and B. Mukherjee, "Miniaturised highly selective bandpass filter with very wide stopband using meander coupled lines," *Electronics Letters*, Vol. 53, No. 13, 889–890, 2017.
17. Gao, X., W. Feng, and W. Che, "Compact ultra-wideband bandpass filter with improved upper stopband using open/shorted stubs," *IEEE Microwave and Wireless Components Letters*, Vol. 27, No. 2, 123–125, Feb. 2017.
18. Li, X., Q. Xia, and J. Zeng, "A compact quadruple-mode ultra-wideband bandpass filter with a broad upper stopband based on transversal-signal interaction concepts," *Progress In Electromagnetics Research Letters*, Vol. 69, 119–125, 2017.
19. Zhu, L., S. Sun, and R. Li, *Microwave Bandpass Filters for Wideband Communications*, 45–46, John Wiley & Sons, Inc. Press, 2012.
20. Jones, E. M. T., "Coupled-strip-transmission-line filters and directional couplers," *IRE Transactions on Microwave Theory and Techniques*, Vol. 4, No. 2, 75–81, 1956.